




Article

Polyaniline/Bi₁₂TiO₂₀ Hybrid System for Cefixime Removal by Combining Adsorption and Photocatalytic Degradation

Oussama Baaloudj ^{1,*} , Nouredine Nasrallah ¹, Hamza Kenfoud ¹ , Khaled Wassim Bourkeb ² and Ahmad K. Badawi ³ 

¹ Laboratory of Reaction Engineering, Faculty of Mechanical Engineering and Process Engineering, USTHB, BP 32, Algiers 16111, Algeria

² Laboratory of Sciences and Industrial Processes Engineering, Department of the Environment Engineering, USTHB, BP 32, Algiers 16111, Algeria

³ Civil Engineering Department, EL-Madina Higher Institute for Engineering and Technology, Giza 12588, Egypt

* Correspondence: obaaloudj@usthb.dz; Tel.: +213-661899266

Abstract: Sillenite catalysts have shown efficient photocatalytic activity for the removal of various pollutants from water in previous studies, thus enhancing their activity by combining them with other materials will be very promising for environmental applications. In this context, an interesting hybrid system containing Polyaniline (PANI) as an adsorbent and Bi₁₂TiO₂₀ (BTO) sillenite as a catalyst was proposed in this work. Cefixime (CFX) has been selected as a pollutant for this study, and its removal was evaluated using PANI (adsorption), PANI and BTO (combined system) and the hybrid system Bi₁₂TiO₂₀/Polyaniline (BTO/PANI). First, the impact of PANI adsorption was investigated on its own; after that, the solution was filtered to separate the adsorbent from the liquid in order to re-treat the solution using photocatalysis (combining adsorption with photocatalysis). At the same time, a similar technique was used involving the hybrid system BTO/PANI. The results show that the hybrid system can remove a very high Cefixime concentration of 30 mg/L, almost 100%, within only 2 h, and this is better than previous investigations. These results indicate that it is possible to combine photocatalysis and adsorption processes to control water pollution.

Keywords: hybrid system; photocatalysis; adsorption; degradation; Cefixime



Citation: Baaloudj, O.; Nasrallah, N.; Kenfoud, H.; Bourkeb, K.W.; Badawi, A.K. Polyaniline/Bi₁₂TiO₂₀ Hybrid System for Cefixime Removal by Combining Adsorption and Photocatalytic Degradation. *ChemEngineering* **2023**, *7*, 4. <https://doi.org/10.3390/chemengineering7010004>

Academic Editor: Luis M. Gandía

Received: 19 August 2022

Revised: 12 October 2022

Accepted: 23 December 2022

Published: 10 January 2023



Copyright: © 2023 by the authors. Licensee MDPI, Basel, Switzerland. This article is an open access article distributed under the terms and conditions of the Creative Commons Attribution (CC BY) license (<https://creativecommons.org/licenses/by/4.0/>).

1. Introduction

Heterogeneous photocatalysis employing semiconductors as catalysts is more effective in environmental applications because they are very effective, simple to make, and employed in a heterogeneous method that allows them to be extracted from water [1,2]. Aside from their ability to produce charge carriers by converting light energy into chemical energy, they also possess other qualities that make them suitable for photocatalytic reactions [3,4]. These include optical and catalytic characteristics [5,6]. Most people agree that TiO₂ and ZnO are among the most photoactive catalysts [7]. However, their drawbacks, such as a high rate of photogenerated electron-hole pair recombination and low irradiation sensitivity because of their wide energy bandgap, limit their applicability [8,9]. It is required to create novel, effective, and multifunctional semiconductors with outstanding photocatalytic activities, suitable photogenerated pair recombination rates, and a narrow bandgap in order to address these challenges. The best core metal ion for semiconductor synthesis for photocatalysis applications are titanium (Ti), bismuth (Bi), zinc (Zn), and tin (Sn) [10,11]. Bismuth semiconductors, especially sillenites, have lately become extremely desirable due to their exceptional chemical stability, powerful light absorption, low pair recombination rate, and low optical bandgap [12–14]. Among sillenites, Bi₁₂TiO₂₀ has shown promising results in various applications in previous studies [15,16].

Even though photocatalysis has proven to be incredibly efficient, there are numerous practical instances where it just cannot be used [12]. Water can contain large amounts of

pollutants, making their removal by photocatalysis very challenging [17]. It is well documented that the pollutants in water can occupy surface active sites available in the catalyst (saturation), resulting in much lower degradation efficiency by inhibiting the reactants from adhering to the catalyst surfaces, such as oxygen and hydrogen [18–23]. Considering the drawbacks and limits of photocatalysis methods, hybrid processes have gained increased attention in an effort to improve process performance. The researchers demonstrated that combining processes reduces the weaknesses in the processes and that the performance of the combined system is superior to that of the individual processes [24,25]. By creating hybrid systems that are highly effective in removing pollutants, energy consumption may be decreased. In recent years, several different combination techniques have been used for the purification and treatment of complex water matrices [26]. Photocatalysis is integrated with physical or chemical processes that have an impact on the chemical kinetics and/or overall efficiency in order to enhance overall performance [27]. These combinations boost efficiency by speeding up discrete processes' reaction times or lowering the price of photocatalysis alone [27–29]. Adsorption can only be effective at large concentrations of contaminants; it could be ineffective at low quantities [30,31]. In contrast, photocatalysis can only function at low concentrations [32,33]. Moreover, adsorption can only remove the pollutant from the water by mass transfer into the adsorbent, where photocatalysis can decompose the pollutant. Therefore, it is very interesting to combine those techniques for water treatment. In addition, another advantage of combining processes is that it can create heterojunction between the materials, which can increase the rate of photoactivity by extending the spectral photo response of wide-band materials such as polymers, which means more energy use and more efficiency [34–36]. Therefore, it is crucial to create systems that have high adsorption capacity as well as strong photocatalytic activity. In this context, combining the sillenites as catalysts with an adsorbent polymer such as polyaniline will be very interesting [37–40]. That is because polyaniline has many advantages in the adsorption process such as a large specific surface area, suitable porous structure, high adsorption capacity and robustness, ease of preparation, and regeneration [41–43].

As already discussed, the combination of processes minimizes their weaknesses of them, and also, the combined system performance is better than each process alone [44]. Furthermore, the combination can reduce energy consumption and cause fewer problems with pollution. In this respect, this work aims to combine adsorption with photocatalysis using the hybrid system Polyaniline/Bi₁₂TiO₂₀. This hybrid catalyst has been tested in order to enhance the removal of the antibiotic Cefixime from water. An adsorption application using the efficient adsorbent polyaniline has been performed. This adsorbent was also combined with a sillenite to produce an efficient hybrid process that is more efficient than photocatalysis alone.

2. Materials and Methods

2.1. Chemicals

Cefixime (C₁₆H₁₅N₅O₇S₂) was taken as a topical example of antibiotics for photocatalytic applications, and it was supplied by the pharmaceutical company Pharmalliance in Algeria. Other chemicals and products used in the synthesis of the materials were bismuth nitrate pentahydrate from Chem-Lab [Bi(NO₃)₃·5H₂O] (98.5%), titanium dioxide from Merck [TiO₂] (99%), nitric acid, ammonium persulfate (NH₄)₂S₂O₈ (Sigma-Aldrich), and Aniline. Polyvinylpyrrolidone (PVP K30) was also supplied by the pharmaceutical company Pharmalliance. Distilled water was used as a solvent. All chemicals have been used as obtained without further purification.

2.2. Synthesis of Bi₁₂TiO₂₀ Sillenite

The sillenite Bi₁₂TiO₂₀ was created using the sol-gel process by combining stoichiometric proportions (1:12 ratio) of [Bi(NO₃)₃·5H₂O] and [TiO₂] in an aqueous solution with a concentration of 20% volume HNO₃ for improved solubilization. Following solubilization, a 15% *w/w* dose of PVP K30 solution was added to the initial solution as a combustion

component. After being concentrated for 24 h by evaporation at 80 °C, the resultant solution was transformed into a yellow gel. This gel was then burned at 200 °C for 6 h to turn it into xerogel. To increase crystallinity and eliminate any leftover carbonated waste from burning, this amorphous xerogel was crushed and then calcinated at 600 °C in the air for 6 h. The calcination duration of 6 h was chosen since it was discovered that calcining the sample for more than 6 h might melt it and cause it to stick in the oven due to the maximum calcination temperature. In addition, the crystallinity was improved and the carbonaceous residue was eliminated from the combustion process by selecting the longest calcination duration [45]. Figure 1 provides a schematic illustration of the sol-gel synthesis procedure.

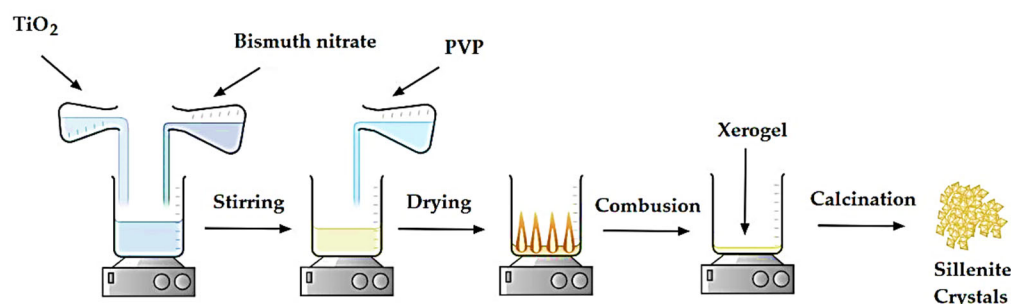


Figure 1. Schematic illustration of the sol-gel synthesis method.

2.3. Synthesis of Polyaniline

Polyaniline (PANI) was synthesized chemically according to the method described in the literature [46]. A total of 0.2 mol of Aniline was dissolved in 200 mL of hydrochloric acid HCl solution (0.5 M). The two solutions were mixed at 0 °C with stirring for 30 min. Then, 200 mL of ammonium persulfate ($(\text{NH}_4)_2\text{S}_2\text{O}_8$ (0.5 M) as an initiator was added dropwise to induce the polymerization reaction, and the reaction was carried out with magnetic stirring. After 4 h, the residue was obtained by filtration using filter paper and washed thoroughly with ethanol and deionized water to remove excess acid and Aniline oligomer, then dried at room temperature for 48 h. Figure 2 represents the diagram of the synthesis.

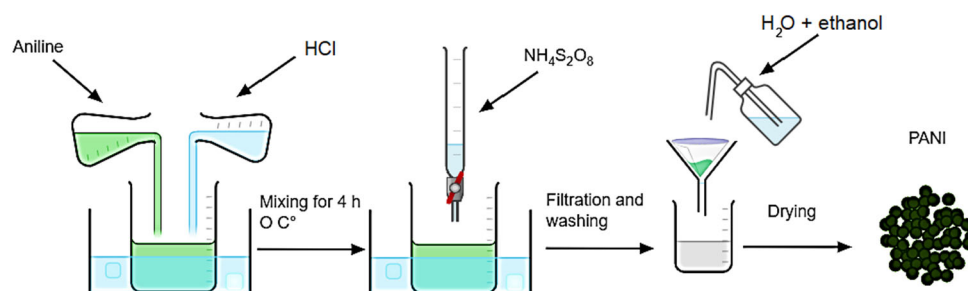


Figure 2. Diagram of the different stages of Polyaniline synthesis.

2.4. Preparation of the Hybrid System BTO/PANI

After obtaining the pure phase of both the catalyst $\text{Bi}_{12}\text{TiO}_{20}$ and the adsorbent Polyaniline, they were mixed by grinding using a pestle in an agate mortar in order to obtain a hybrid system (catalyst/adsorbent). The mixture was constantly mixed until a homogenous powder was formed. Preliminary tests have been performed in order to find the optimal ratio between the catalyst and the adsorbent, by changing the ratio between BTO/PANI: 100% PANI, 75%/25%, 50%/50%, 25%/75% and 100% BTO. The tests were all in the same conditions of a pH of 6, 200 mL of 30 mg/L CFX concentration, 2 g/L of total added materials mass (PANI + BTO), and under UV irradiation. The optimal ratio was found to be 75%/25%. A schematic of the BTO/PANI hybrid system's preparation is shown in Figure 3.

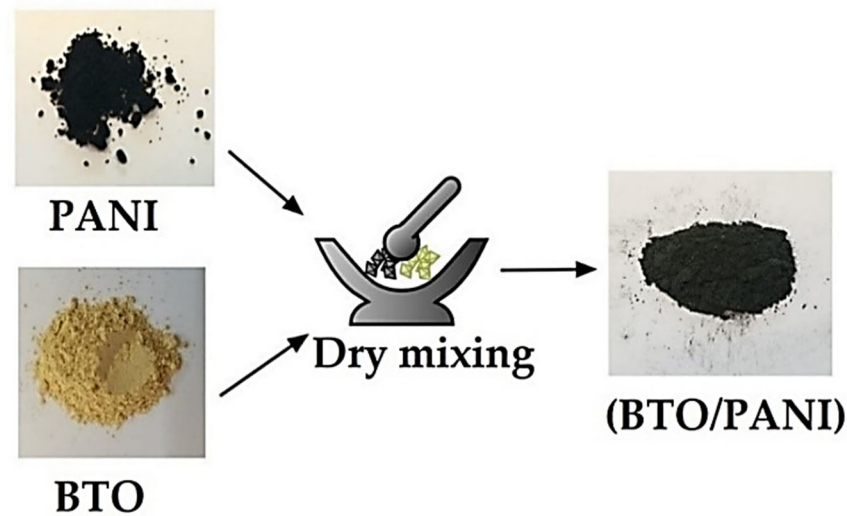


Figure 3. Schematic illustration of the preparation of the BTO/PANI hybrid system.

2.5. Characterization

The materials were characterized by XRD analysis to confirm the obtaining of the phases. XRD analysis was performed by PW 1730 Philips with monochromatic radiation with $\lambda = 0.15417$ nm. Other characterization techniques are provided in previous studies for BTO [15,47] and for PANI [46,48,49].

2.6. Hybrid and Combined Experiments

The removal of CFX was also evaluated using PANI, PANI coupled with BTO, and the hybrid PANI/BTO material, in order to enhance the removal rates. First of all, the effect of PANI adsorption alone was tested; 200 mL of 30 mg/L CFX was prepared with pH = 6, and 0.5 g/L of the PANI was added and magnetically stirred in the dark condition. Then, the adsorption rate started to be analyzed directly after adding the PANI to the solution because adsorption is a rapid process. After reaching the adsorption equilibrium, the solution was filtered to separate the adsorbent from the liquid; this was to re-treat the solution using photocatalysis (combining adsorption with photocatalysis), as shown in Figure 4a. The obtained solution was re-treated using the BTO catalyst with a concentration of 1.5 g/L (optimal). The suspension was irradiated using ultraviolet light (UVA). A similar procedure (Figure 4b) was adopted using the hybrid system BTO/PANI. A total of 100 mL of 30 mg/L CFX was prepared with pH = 6. Then, 2 g/L of the hybrid system (0.5 g/L of PANI and 1.5 g/L of BTO catalyst) was added and magnetically stirred under irradiation using ultraviolet light UVA 24 W (Philips PL/L).

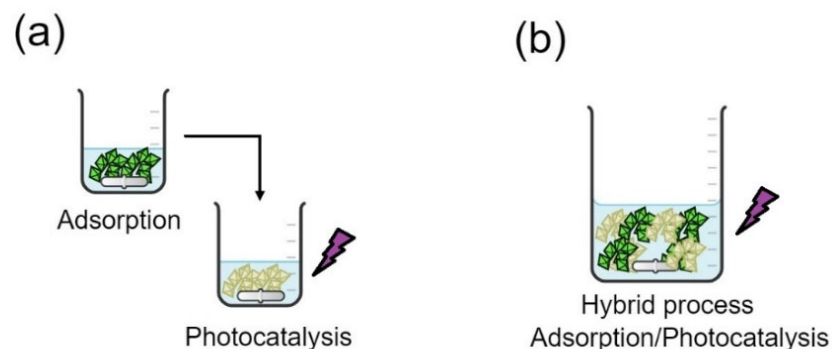


Figure 4. (a) Combined and (b) hybrid processes for Cefixime removal.

2.7. Analysis Method

The concentration of CFX was determined by following the absorbance wavelength 288 nm corresponding to the molecule CFX using a UV-visible spectrophotometer (OPTI-ZEN, UV-3220UV). The analysis was performed using UV-visible spectrometry since it is quick and only has a little inaccuracy when compared to HPLC analysis [47]. To remove the suspended particles from the liquid, the solution aliquots were centrifuged for 15 min at a speed of 3000 rpm. The following equation was used to compute the degradation rate:

$$\text{Removal efficiency \%} = \frac{(C_0 - C_t)}{C_0} \times 100\% \quad (1)$$

where C_0 is the initial concentration of the CFX and C_t is the concentration after irradiation at the time (t).

A calibration curve was constructed by spectrophotometry to show the absorbance of a solution as a function of the CFX concentration. The concentrations of CFX employed in the trials given in this study vary from 5 mg/L to 30 mg/L. The dilution was made to prepare a series of four concentrations defeated (5 mg/L, 10 mg/L, 20 mg/L, 30 mg/L); then, the absorbance of each solution was measured. The 0 mg/L (blank) was measured by a tank containing distilled water. Figure 5 shows the calibration curve as well as the associated UV spectrum of different concentrations. The calibration curve is linear over the chosen concentration interval, so the Beer–Lambert law is verified to determine the molar extinction coefficient. The Beer–Lambert is generally presented as the next relation.

$$\text{Absorbance} = \epsilon_{\lambda} \cdot L \cdot C \quad (2)$$

where Absorbance is the absorbance or optical density at a wavelength λ , ϵ_{λ} is the molar extinction coefficient, its value depends on the temperature and the wavelength of the incident light, L is the thickness of the cell, and C is the attenuating species concentration in the solution (mg/L).

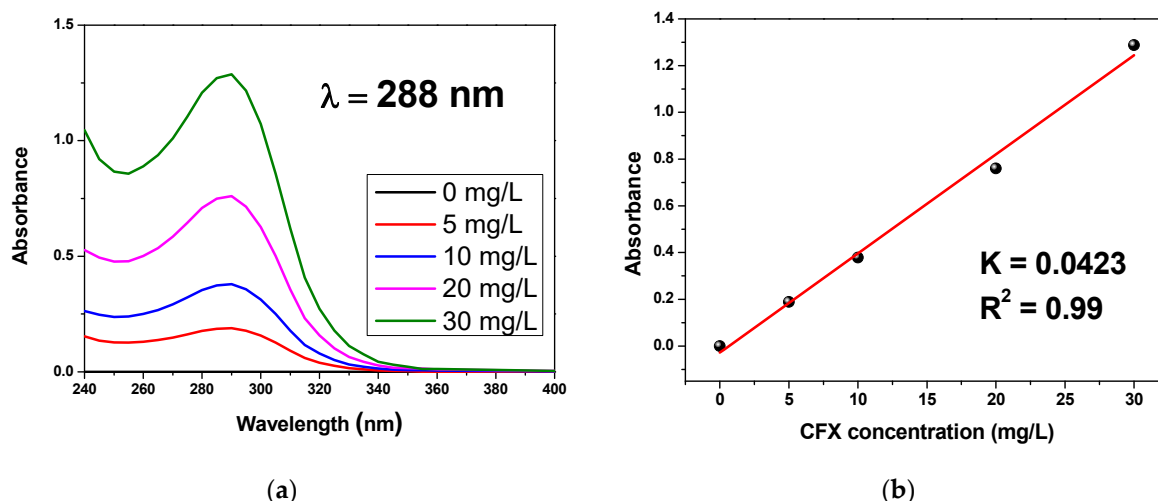


Figure 5. (a) The UV spectrum of various concentrations and (b) the calibration curve.

3. Results and Discussion

3.1. Phase Identification

The X-ray diffraction patterns of the catalyst BTO and the polymer PANI at room temperature are shown in Figure 6. For the polymer PANI, it shows five main characteristic diffraction peaks with a 2θ value at 9.1, 14.4, 20.9, 25.5, and 27.4, respectively, which are very similar to that reported in the literature [50]. The polymer is semi-crystalline in nature because the unit shows sharp peaks due to the presence of benzenoid and quinonoid groups in the polyaniline [51]. The large width (2θ) of the majority of these peaks represents the

degree of orientation of the polymer chains due to long PANI chains and a more ordered structure and also shows good agreement with those in the literature [52]. For the catalyst BTO, all peaks are cubic-type sillenite $\text{Bi}_{12}\text{TiO}_{20}$ with space group $I23$ according to the specifications PDF-340097 and ICDD N° 98-006-2302 [53].

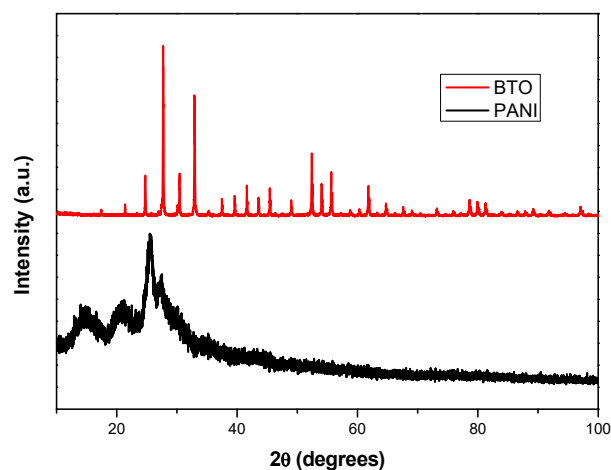


Figure 6. XRD diffractogram of BTO as well as PANI.

3.2. Combined and Hybrid Processes for Cefixime Removal in a Batch Reactor

The removal of Cefixime was evaluated using PANI (adsorption), PANI and then with BTO (combined system), and the hybrid PANI/BTO material (hybrid system) in order to enhance the performance of the removal. First, the impact of PANI adsorption was investigated on its own; after that, the solution was filtered to separate the adsorbent from the liquid in order to re-treat the solution using photocatalysis (combining adsorption with photocatalysis). At the same time, a similar technique was used involving the hybrid system BTO/PANI.

3.2.1. Cefixime Removal Using Adsorption

First of all, the effect of PANI adsorption alone was tested; with a pH of 6, 200 mL of 30 mg/L CFX was produced, and 0.5 g/L of PANI was added and magnetically swirled in the dark. The adsorbent dose of 0.5 g/L was selected as an ideal adsorbent dose and the most convenient for the adsorption process, first of all, based on the optimal quantities for the hybrid system, which are 0.5 g/L PANI and 1.5 g/L BTO, as it was found in the primary studies. Therefore, the combined process will follow the same quantities of materials in the hybrid process in order to compare them. Another reason that this adsorbent dose is the most convenient in the combined process is that it has a good adsorption efficiency and does not remove a large CFX concentration, leaving the opportunity for the next step of photocatalysis to remove the rest. A 1g/L dose was indeed found to be the optimal adsorbent dose with an efficiency of 89.65% in 1 h for the adsorption process alone; however, a 0.5 g/L dose was more effective in the hybrid process because of the opacity of the solution. Whereas the adsorbent dose needs to be as low as possible to not increase the opacity of the solution, which decreases the light penetration and decreases the photocatalytic activity due to a scattering effect for an expansion of the dose because of the dark color of the adsorbent.

The adsorption capacity of CFX adsorbed by polyaniline in Figure 7a was calculated according to the following equation [54]:

$$q = \frac{(C_o - C_t) \times V}{m} \quad (3)$$

where q is the adsorption capacity (mg/g), C_o is the initial concentration, C_t is the concentration at time (t), m is the mass of the adsorbent (0.1 g), and V is the volume of the solution (0.2 L).

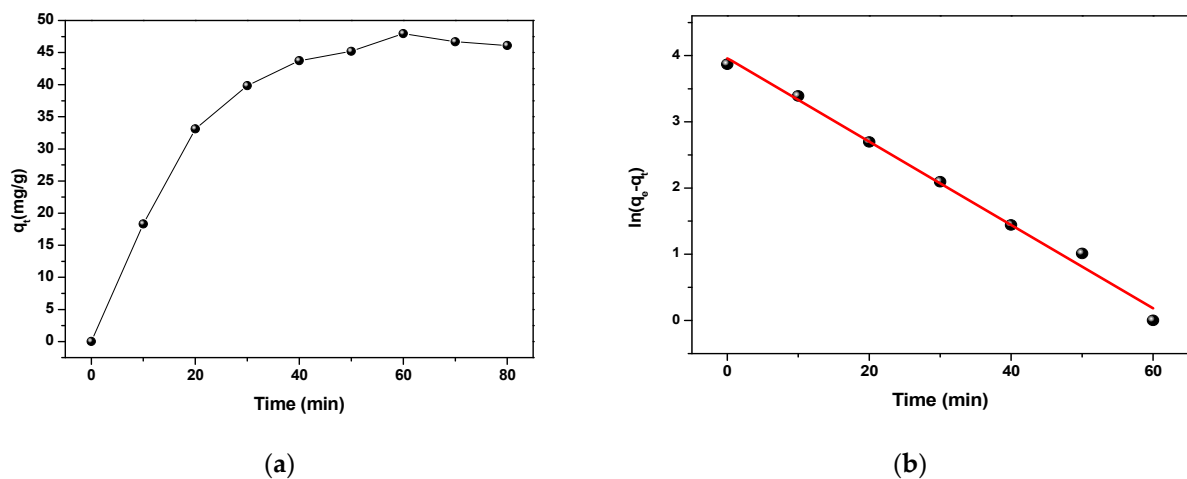


Figure 7. (a) The adsorption capacity of CFX adsorbed by PANI and (b) the pseudo-first-order kinetic plot.

Lagergren has presented the equation for the pseudo-first-order kinetics of adsorption in the following linear form [54,55]:

$$\ln(q_e - q_t) = \ln(q_e) - Kt \quad (4)$$

where q_e (mg/g) and q_t mean the adsorption capacity of the adsorbent at equilibrium and at time t (min), respectively, and K ($6.29 \times 10^{-2} \text{ min}^{-1}$) is the pseudo-first-order rate constant (min^{-1}), which was determined by the slope and the order at the origin, respectively, from the plot of $\ln(q_e - q_t)$ as a function of time shown in Figure 7b.

CFX adsorption is also presented as efficiency in Figure 8a. As can be seen, the PANI showed an efficient removal for CFX with an efficiency of 76.83% within 70 min. The decrease happened at the point between 60 and 70 min because the adsorbent has achieved equilibrium between the adsorption and desorption.

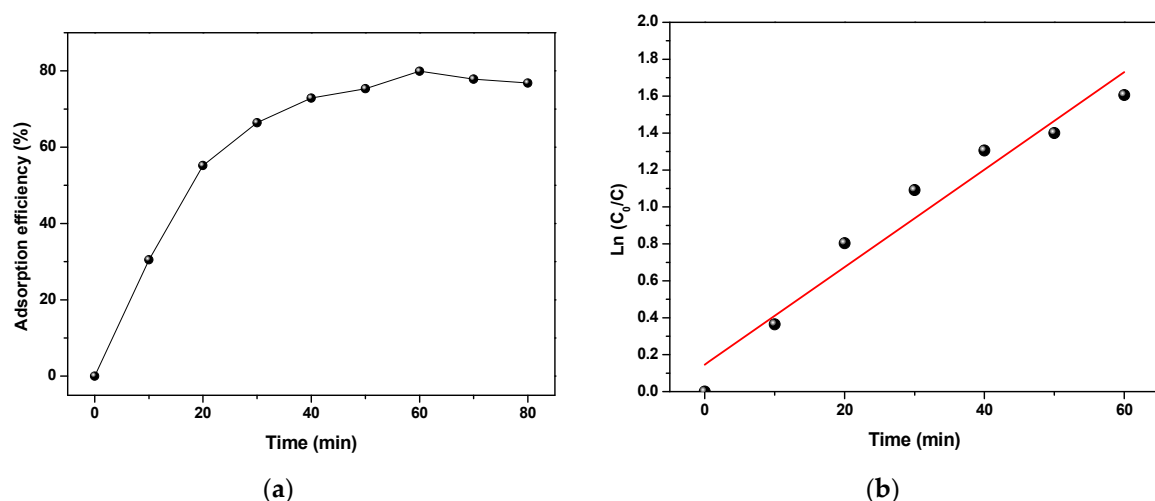


Figure 8. (a) CFX removal by adsorption using PANI and (b) the pseudo-first-order kinetic plot.

The kinetics of the adsorption (Figure 8b) was studied using the following pseudo-first-order model of the photocatalysis process (Equation (5)) in order to compare its kinetic constant with the combined and hybrid systems.

$$\ln \frac{C_0}{C} = k(t) \quad (5)$$

where C and C_0 are the concentrations (mg/L) of CFX at a time, t and $t = 0$, respectively. k is the constant called pseudo-first-order rate constant, expressed in min^{-1} and determined from the slope of the curve drawn between $\ln \frac{C_0}{C}$ and light irradiation time.

Modeling results of the adsorption efficiency of PANI on CFX were in accordance with the first-order kinetic reaction and it was validated by the R^2 value (0.9448). The k constant was calculated to be $2.64 \times 10^{-2} \text{ min}^{-1}$. This operation was repeated in light conditions using a UV lamp. However, the same removal efficiency for CFX was obtained in dark conditions. This means that only adsorption has happened in the presence of PANI alone under UV irradiation.

3.2.2. Cefixime Removal Using Adsorption Combined with Photocatalysis

The previous adsorption process was combined with the photocatalysis process using the efficient BTO catalyst, as it showed in previous parts an efficient removal of large types of pollutants. An adsorption experiment, the same as the previous part, was tested in the same conditions. After adsorption, the solution was filtered to separate the adsorbent from the liquid; this was to re-treat the solution using photocatalysis (combining adsorption with photocatalysis). The results are presented in Figure 9a. After adsorption, when an equilibrium between the adsorption and desorption was achieved, a removal efficiency for CFX of 76.83% was reached using PANI. After that, the photocatalysis starts by removing the adsorbent and adding the catalyst. As can be seen, the remaining concentration of CFX was eliminated using photocatalysis with a removal efficiency of 94.64% within 260 min. This combined system has shown a very efficient removal for high CFX concentration (30 mg/L).

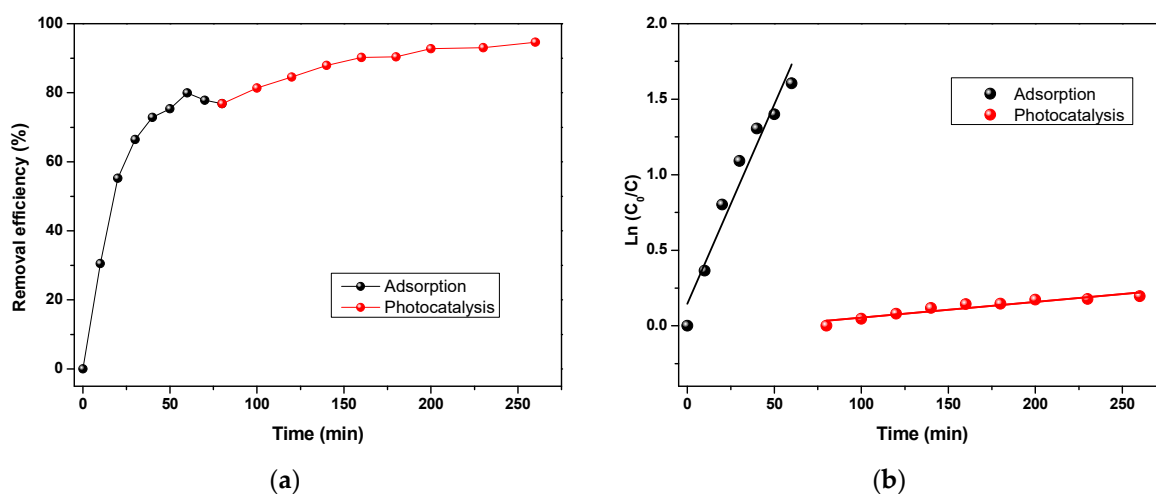


Figure 9. (a) CFX removal by adsorption combined with photocatalysis and (b) the pseudo-first-order kinetic plot.

The reaction kinetics of both adsorption and photocatalysis on the CFX removal (Figure 9b) were studied using a pseudo-first-order model (Equation (5)). Modeling results of the photocatalysis and adsorption efficiency of BTO and PANI on CFX were all following the first-order kinetic reaction and they were validated by the R^2 values (0.884 and 0.9448, respectively). The k constants were calculated to be $2.64 \times 10^{-2} \text{ min}^{-1}$ and $1.04 \times 10^{-3} \text{ min}^{-1}$ for adsorption and photocatalysis, respectively.

3.2.3. Cefixime Removal Using Adsorption/Photocatalysis Hybrid Process

A similar procedure as the previous part was adopted using the hybrid system BTO/PANI. A total of 100 mL of 30 mg/L CFX was prepared with $\text{pH} = 6$. An amount of 2 g/L of the hybrid system with a ratio of 75% BTO/25% PANI (0.5 g/L of PANI and 1.5 g/L of BTO catalyst) was added and magnetically stirred under irradiation using ultraviolet light UVA 24 W (Philips PL/L).

The results are presented in Figure 10a. As can be seen, the CFX removal was more rapid and efficient than in the previous experiments (adsorption alone, photocatalysis alone, and both combined processes). The efficiency has achieved 94.95% within only 110 min; this was unexpected. It was expected that there is an inhibition effect between adsorption and photocatalysis; however, it was found that there is a synergistic effect between them. This can be explained by the fact that the adsorbent PANI has a semiconductor behavior; however, it does not work alone under UV irradiation. In a previous work, the bandgap of the catalyst BTO was found to be 2.9 eV [47]. By adding a narrow bandgap catalyst, a heterogeneous effect occurred between the BTO catalyst and PANI, increasing the efficiencies of these materials and creating a more efficient system than both alone. Whereas recent studies have demonstrated that hetero-systems can accelerate photoactivity by broadening the spectral optical response to a wideband material, as is the case here [46,56–58]. Another aspect that can be a reason for this increase is the fine nature of the mixture, where the polyaniline is always agglomerated when it is alone; however, by mixing it with the catalyst BTO, it obtains a fine nature. This has a major role in increasing the adsorption effect by increasing the specific surface area of the adsorbent.

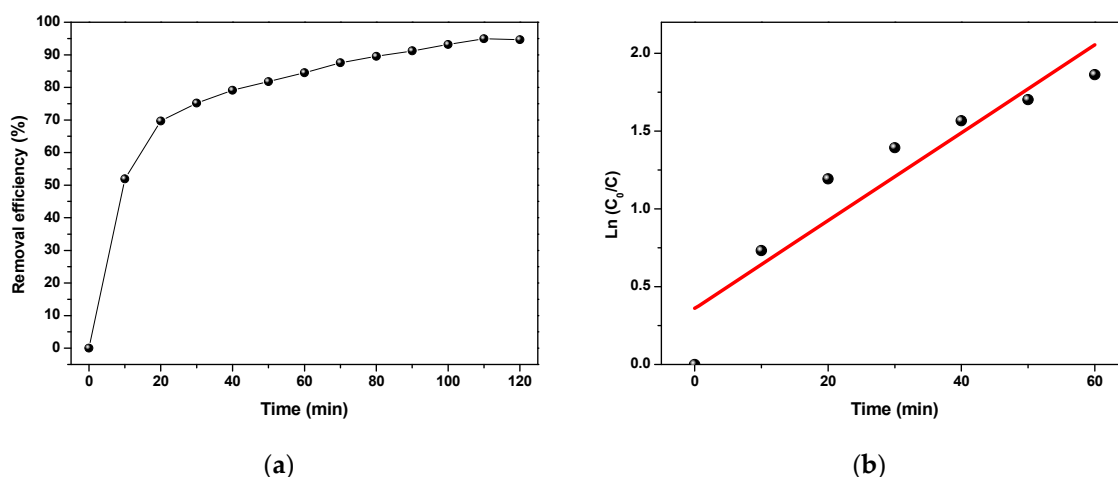


Figure 10. (a) CFX removal by adsorption and photocatalysis using BTO/PANI hybrid system and (b) the pseudo-first-order kinetic plot.

The reaction kinetics of this hybrid system on the CFX was studied using a pseudo-first-order model (Figure 10b) using (Equation (5)). Modeling results followed the first-order kinetic reaction and it was validated by the R^2 value (0.943). The k constant was calculated to be $2.822 \times 10^{-2} \text{ min}^{-1}$, and it was found to be higher than the previous constants (adsorption, photocatalysis, and combined process). The higher the rate constant, the more efficient and quicker the degradation; this proves the previous interpretations and conclusions.

Based on previous parts and recent studies [59], the mechanism, electron, and hole transport pathways of the BTO/PANI system in CFX degradation under UV light can be constructed. Previous results indicate that $\text{O}_2^{\bullet-}$ and $\bullet\text{OH}$ radicals are vital active species in CFX degradation. Under UV light, the BTO catalyst adsorbs light and generates electrons and holes. Then, the generated electrons are moved from the valence band (VB) to the conduction band (CB) of BTO and the highest occupied molecular orbital (HOMO) of PANI to the lowest unoccupied molecular orbital (LUMO) of PANI through π - π^* transitions [59].

Therefore, the excited BTO electrons are readily injected into the CB of PANI or the electrons are directly reacting with oxygen to yield active species of superoxide radicals. On the other hand, the PANI exchanges those electrons through holes in the BTO catalyst. The exchanged electron-hole pairs (e^- and h^+) between the BTO catalyst and PANI generates then the active species $\bullet\text{OH}$ and $\text{O}_2^{\bullet-}$. Whereas the radical $\bullet\text{OH}$ is generated by oxidation of H_2O adsorbed on the catalyst surface using h^+ in the valence band (V_B), and the radical $\text{O}_2^{\bullet-}$ is produced by reduction of O_2 adsorbed on the catalyst surface using e^- in the

conduction band (C_B) [33]. The obtained active species $\bullet OH$ and $O_2^{\bullet -}$ are highly reactive reagents in a chemical reaction, so both can perform a chemical reduction or oxidation reaction upon contact with organic pollutants, which then causes their decomposition into small particles.

The next reactions could describe the mechanism of CFX photodegradation over the BTO/PANI hybrid system. Figure 11 shows a schematic depiction of the proposed mechanism.

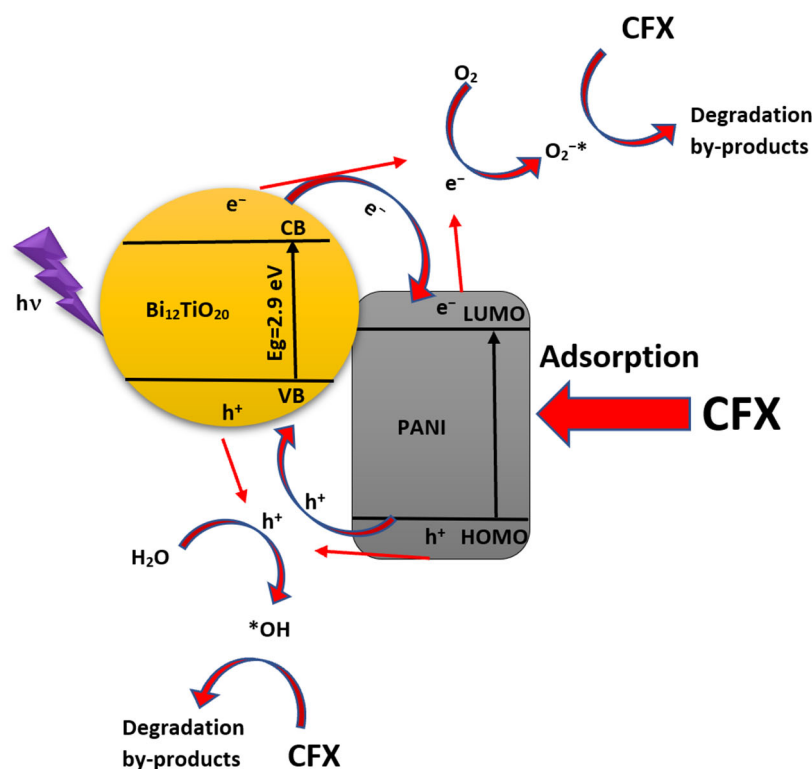
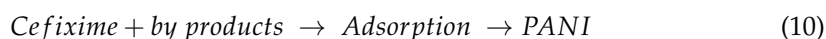
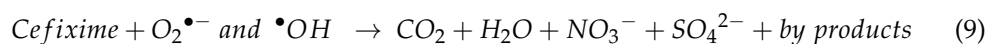
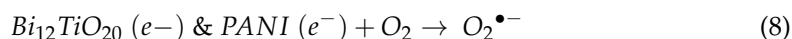
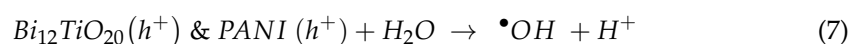


Figure 11. Possible photocatalytic/adsorption CFX removal mechanism into the hybrid system $Bi_{12}TiO_{20}/PANI$.

4. Conclusions

This work aims to test hybrid systems in order to enhance the removal efficiency of the photocatalytic process. Starting with the characterization of the materials, the XRD has confirmed the obtaining of the phases of BTO and PANI after synthesis. The sillenite $Bi_{12}TiO_{20}$ was taken as a typical example for this application due to its efficiencies and originalities. Combining this sillenite as a catalyst with an adsorbent polymer such as polyaniline was interesting as a hybrid/combined system; for that, it was handled. The efficiency of those materials has been tested for the removal of CFX. The polymer PANI has shown alone an efficient removal of CFX by adsorption with an efficiency of 76.83% within 70 min. An interesting enhancement in removing Cefixime was obtained using the hybrid system $Bi_{12}TiO_{20}/Polyaniline$, where it almost removes a CFX concentration of 30 mg/L within only 2 h, which is very high efficiency.

Author Contributions: Conceptualization, O.B. and H.K.; methodology, O.B.; software, O.B.; validation, O.B.; formal analysis, K.W.B.; investigation, O.B.; resources, N.N.; data curation, O.B.; writing—original draft preparation, O.B., H.K. and A.K.B.; writing—review and editing, O.B., A.K.B. and H.K.; visualization, O.B. and K.W.B.; supervision, O.B. All authors have read and agreed to the published version of the manuscript.

Funding: This work was financially supported by the Faculties of Mechanical Engineering and Process Engineering.

Data Availability Statement: Not applicable.

Conflicts of Interest: The authors declare no conflict to interest.

References

1. Noh, T.H.; Hwang, S.W.; Kim, J.U.; Yu, H.K.; Seo, H.; Ahn, B.; Kim, D.W.; Cho, I.S. Optical properties and visible light-induced photocatalytic activity of bismuth sillenites ($\text{Bi}_{12}\text{XO}_{20}$, X = Si, Ge, Ti). *Ceram. Int.* **2017**, *43*, 12102–12108. [\[CrossRef\]](#)
2. Hou, D.; Hu, X.; Wen, Y.; Shan, B.; Hu, P.; Xiong, X.; Qiao, Y.; Huang, Y. Electrospun sillenite $\text{Bi}_{12}\text{MO}_{20}$ (M = Ti, Ge, Si) nanofibers: General synthesis, band structure, and photocatalytic activity. *Phys. Chem. Chem. Phys.* **2013**, *15*, 20698–20705. [\[CrossRef\]](#) [\[PubMed\]](#)
3. Benrighi, Y.; Nasrallah, N.; Chaabane, T.; Belkacemi, H.; Bourkeb, K.W.; Kenfoud, H.; Baaloudj, O. Characterization and application of the spinel CuCr_2O_4 synthesized by sol–gel method for sunset yellow photodegradation. *J. Sol-Gel Sci. Technol.* **2022**, *101*, 390–400. [\[CrossRef\]](#)
4. Fosso-Kankeu, E.; Pandey, S.; Ray, S.S. Photocatalysts in advanced oxidation processes for wastewater treatment. In *Photocatalysts in Advanced Oxidation Processes for Wastewater Treatment*; John Wiley & Sons: Hoboken, NJ, USA, 2020; ISBN 9781119631415.
5. Akerdi, A.G.; Bahrami, S.H. Application of heterogeneous nano-semiconductors for photocatalytic advanced oxidation of organic compounds: A review. *J. Environ. Chem. Eng.* **2019**, *7*, 103283. [\[CrossRef\]](#)
6. Jaffari, Z.H.; Lam, S.M.; Sin, J.C.; Zeng, H.; Mohamed, A.R. Magnetically recoverable Pd-loaded BiFeO_3 microcomposite with enhanced visible light photocatalytic performance for pollutant, bacterial and fungal elimination. *Sep. Purif. Technol.* **2020**, *236*, 116195. [\[CrossRef\]](#)
7. Gebre, S.H.; Sendeku, M.G. New frontiers in the biosynthesis of metal oxide nanoparticles and their environmental applications: An overview. *SN Appl. Sci.* **2019**, *1*, 928. [\[CrossRef\]](#)
8. Yao, W.F.; Wang, H.; Xu, X.H.; Zhang, Y.; Yang, X.N.; Shang, S.X.; Liu, Y.H.; Zhou, J.T.; Wang, M. Characterization and photocatalytic properties of Ba doped $\text{Bi}_{12}\text{TiO}_{20}$. *J. Mol. Catal. A Chem.* **2003**, *202*, 305–311. [\[CrossRef\]](#)
9. He, C.; Gu, M. Photocatalytic activity of bismuth germanate $\text{Bi}_{12}\text{GeO}_{20}$ powders. *Scr. Mater.* **2006**, *54*, 1221–1225. [\[CrossRef\]](#)
10. Shahzad, W.; Badawi, A.K.; Rehan, Z.A.; Khan, A.M.; Khan, R.A.; Shah, F.; Ali, S.; Ismail, B. Enhanced visible light photocatalytic performance of $\text{Sr}_{0.3}(\text{Ba},\text{Mn})_{0.7}\text{ZrO}_3$ perovskites anchored on graphene oxide. *Ceram. Int.* **2022**, *48*, 24979–24988. [\[CrossRef\]](#)
11. Qiao, X.; Pu, Y.; Li, Y.; Huang, Y.; Cheng, H.; Seo, H.J. Structural characteristics and photocatalytic ability of vanadate-sillenite $\text{Bi}_{25}\text{VO}_{40}$ nanoparticles. *Powder Technol.* **2016**, *287*, 277–284. [\[CrossRef\]](#)
12. Baaloudj, O.; Kenfoud, H.; Badawi, A.K.; Assadi, A.A.; Jerry, A.E.; Assadi, A.A.; Amrane, A. Bismuth Sillenite Crystals as Recent Photocatalysts for Water Treatment and Energy Generation: A Critical Review. *Catalysts* **2022**, *12*, 500. [\[CrossRef\]](#)
13. Zhu, X.; Zhang, J.; Chen, F. Study on visible light photocatalytic activity and mechanism of spherical $\text{Bi}_{12}\text{TiO}_{20}$ nanoparticles prepared by low-power hydrothermal method. *Appl. Catal. B Environ.* **2011**, *102*, 316–322. [\[CrossRef\]](#)
14. Tho, N.T.M.; Khanh, D.N.N.; Thang, N.Q.; Lee, Y.I.; Phuong, N.T.K. Novel reduced graphene oxide/ ZnBi_2O_4 hybrid photocatalyst for visible light degradation of 2,4-dichlorophenoxyacetic acid. *Environ. Sci. Pollut. Res.* **2020**, *27*, 11127–11137. [\[CrossRef\]](#)
15. Baaloudj, O.; Badawi, A.K.; Kenfoud, H.; Benrighi, Y.; Hassan, R.; Nasrallah, N.; Assadi, A.A. Techno-economic studies for a pilot-scale $\text{Bi}_{12}\text{TiO}_{20}$ based photocatalytic system for pharmaceutical wastewater treatment: From laboratory studies to commercial-scale applications. *J. Water Process Eng.* **2022**, *48*, 102847. [\[CrossRef\]](#)
16. Zhang, X.; Zhang, L.; Hu, J.S.; Pan, C.L.; Hou, C.M. Facile hydrothermal synthesis of novel $\text{Bi}_{12}\text{TiO}_{20}$ - Bi_2WO_6 heterostructure photocatalyst with enhanced photocatalytic activity. *Appl. Surf. Sci.* **2015**, *346*, 33–40. [\[CrossRef\]](#)
17. Ibadon, A.O.; Fitzpatrick, P. Heterogeneous photocatalysis: Recent advances and applications. *Catalysts* **2013**, *3*, 189–218. [\[CrossRef\]](#)
18. Choi, J.; Lee, H.; Choi, Y.; Kim, S.; Lee, S.; Lee, S.; Choi, W.; Lee, J. Heterogeneous photocatalytic treatment of pharmaceutical micropollutants: Effects of wastewater effluent matrix and catalyst modifications. *Appl. Catal. B Environ.* **2014**, *147*, 8–16. [\[CrossRef\]](#)
19. Shafaei, A.; Nikazar, M.; Arami, M. Photocatalytic degradation of terephthalic acid using titania and zinc oxide photocatalysts: Comparative study. *Desalination* **2010**, *252*, 8–16. [\[CrossRef\]](#)
20. Song, S.; Xu, L.; He, Z.; Ying, H.; Chen, J.; Xiao, X.; Yan, B. Photocatalytic degradation of C.I. Direct Red 23 in aqueous solutions under UV irradiation using $\text{SrTiO}_3/\text{CeO}_2$ composite as the catalyst. *J. Hazard. Mater.* **2008**, *152*, 1301–1308. [\[CrossRef\]](#) [\[PubMed\]](#)
21. Behnajady, M.A.; Modirshahla, N.; Hamzavi, R. Kinetic study on photocatalytic degradation of C.I. Acid Yellow 23 by ZnO photocatalyst. *J. Hazard. Mater.* **2006**, *133*, 226–232. [\[CrossRef\]](#) [\[PubMed\]](#)

22. Al-ekabi, H.; Serpone, N.; Pelizzetti, E.; Minero, C.; Fox, M.A.; Draper, R.B. Kinetic Studies in Heterogeneous Photocatalysis. 2. TiO_2 -Mediated Degradation of 4-Chlorophenol Alone and in a Three-Component Mixture of 4-Chlorophenol, 2,4-Dichlorophenol, and 2,4,5-Trichlorophenol in Air-Equilibrated Aqueous Media. *Langmuir* **1989**, *5*, 250–255. [\[CrossRef\]](#)
23. Akyol, A.; Yatmaz, H.C.; Bayramoglu, M. Photocatalytic decolorization of Remazol Red RR in aqueous ZnO suspensions. *Appl. Catal. B Environ.* **2004**, *54*, 19–24. [\[CrossRef\]](#)
24. Berardinelli, A.; Hamrouni, A.; Dirè, S.; Ceccato, R.; Camera-Roda, G.; Ragni, L.; Palmisano, L.; Parrino, F. Features and application of coupled cold plasma and photocatalysis processes for decontamination of water. *Chemosphere* **2021**, *262*, 128336. [\[CrossRef\]](#) [\[PubMed\]](#)
25. Taranto, J.; Frochot, D.; Pichat, P. Combining cold plasma and TiO_2 photocatalysis to purify gaseous effluents: A preliminary study using methanol-contaminated air. *Ind. Eng. Chem. Res.* **2007**, *46*, 7611–7614. [\[CrossRef\]](#)
26. Cionti, C.; Pargoletti, E.; Falletta, E.; Bianchi, C.L.; Meroni, D.; Cappelletti, G. Combining pH-triggered adsorption and photocatalysis for the remediation of complex water matrices. *J. Environ. Chem. Eng.* **2022**, *10*, 108468. [\[CrossRef\]](#)
27. Abou Saoud, W.; Assadi, A.A.; Guiza, M.; Bouzaza, A.; Aboussaoud, W.; Ouederni, A.; Soutrel, I.; Wolbert, D.; Rtimi, S. Study of synergetic effect, catalytic poisoning and regeneration using dielectric barrier discharge and photocatalysis in a continuous reactor: Abatement of pollutants in air mixture system. *Appl. Catal. B Environ.* **2017**, *213*, 53–61. [\[CrossRef\]](#)
28. Assadi, A.A.; Loganathan, S.; Tri, P.N.; Gharib-Abou Ghaida, S.; Bouzaza, A.; Tuan, A.N.; Wolbert, D. Pilot scale degradation of mono and multi volatile organic compounds by surface discharge plasma/ TiO_2 reactor: Investigation of competition and synergism. *J. Hazard. Mater.* **2018**, *357*, 305–313. [\[CrossRef\]](#)
29. Assadi, A.A.; Bouzaza, A.; Soutrel, I.; Petit, P.; Medimagh, K.; Wolbert, D. A study of pollution removal in exhaust gases from animal quartering centers by combining photocatalysis with surface discharge plasma: From pilot to industrial scale. *Chem. Eng. Process. Process Intensif.* **2017**, *111*, 1–6. [\[CrossRef\]](#)
30. Ebrahimian Pirbazari, A.; Saberikhah, E.; Badrouh, M.; Emami, M.S. Alkali treated Foumanat tea waste as an efficient adsorbent for methylene blue adsorption from aqueous solution. *Water Resour. Ind.* **2014**, *6*, 64–80. [\[CrossRef\]](#)
31. Dickey, F.H. Specific adsorption. *J. Phys. Chem.* **1955**, *59*, 695–707. [\[CrossRef\]](#)
32. Chen, F.; Liu, Z.; Liu, Y.; Fang, P.; Dai, Y. Enhanced adsorption and photocatalytic degradation of high-concentration methylene blue on Ag_2O -modified TiO_2 -based nanosheet. *Chem. Eng. J.* **2013**, *221*, 283–291. [\[CrossRef\]](#)
33. Baaloudj, O.; Assadi, I.; Nasrallah, N.; El, A.; Khezami, L. Simultaneous removal of antibiotics and inactivation of antibiotic-resistant bacteria by photocatalysis: A review. *J. Water Process Eng.* **2021**, *42*, 102089. [\[CrossRef\]](#)
34. Belaissa, Y.; Nibou, D.; Assadi, A.A.; Bellal, B.; Trari, M. A new hetero-junction p-CuO/n-ZnO for the removal of amoxicillin by photocatalysis under solar irradiation. *J. Taiwan Inst. Chem. Eng.* **2016**, *68*, 254–265. [\[CrossRef\]](#)
35. Boumaza, S.; Bellal, B.; Trari, M. Iodide ion photooxidation on the hetero-system WS_2/TiO_2 prepared by sol-gel. *React. Kinet. Mech. Catal.* **2016**, *118*, 439–450. [\[CrossRef\]](#)
36. Boutra, B.; Güy, N.; Özacar, M.; Trari, M. Magnetically separable $\text{MnFe}_2\text{O}_4/\text{TA}/\text{ZnO}$ nanocomposites for photocatalytic degradation of Congo Red under visible light. *J. Magn. Magn. Mater.* **2020**, *497*, 165994. [\[CrossRef\]](#)
37. Hamdy, M.S.; Abd-Rabboh, H.S.M.; Benaissa, M.; Al-Metwaly, M.G.; Galal, A.H.; Ahmed, M.A. Fabrication of novel polyaniline/ ZnO heterojunction for exceptional photocatalytic hydrogen production and degradation of fluorescein dye through direct Z-scheme mechanism. *Opt. Mater.* **2021**, *117*, 111198. [\[CrossRef\]](#)
38. Feizpoor, S.; Habibi-Yangjeh, A.; Yubuta, K.; Vadivel, S. Fabrication of $\text{TiO}_2/\text{CoMoO}_4/\text{PANI}$ nanocomposites with enhanced photocatalytic performances for removal of organic and inorganic pollutants under visible light. *Mater. Chem. Phys.* **2019**, *224*, 10–21. [\[CrossRef\]](#)
39. Soltani, H.; Belmokhtar, A.; Zeggai, F.Z.; Benyoucef, A.; Bousalem, S.; Bachari, K. Copper(II) Removal from Aqueous Solutions by PANI-Clay Hybrid Material: Fabrication, Characterization, Adsorption and Kinetics Study. *J. Inorg. Organomet. Polym. Mater.* **2019**, *29*, 841–850. [\[CrossRef\]](#)
40. Wang, W.; Song, J.; Kang, Y.; Chai, D.; Zhao, R.; Lei, Z. Sm_2O_3 embedded in nitrogen doped carbon with mosaic structure: An effective catalyst for oxygen reduction reaction. *Energy* **2017**, *133*, 115–120. [\[CrossRef\]](#)
41. Wang, N.; Chen, J.; Wang, J.; Feng, J.; Yan, W. Removal of methylene blue by Polyaniline/ TiO_2 hydrate: Adsorption kinetic, isotherm and mechanism studies. *Powder Technol.* **2019**, *347*, 93–102. [\[CrossRef\]](#)
42. Kumar Sharma, A.; Kumar Jain, P.; Vyas, R.; Mathur, V.; Kumar Jain, V. Synthesis, characterization and study of optical property of $(\text{PANI})_{1-x}(\text{MWCNT})_x$ nanocomposites. *Mater. Today Proc.* **2021**, *38*, 1214–1217. [\[CrossRef\]](#)
43. Shirmardi, A.; Teridi, M.A.M.; Azimi, H.R.; Basirun, W.J.; Jamali-Sheini, F.; Yousefi, R. Enhanced photocatalytic performance of ZnSe/PANI nanocomposites for degradation of organic and inorganic pollutants. *Appl. Surf. Sci.* **2018**, *462*, 730–738. [\[CrossRef\]](#)
44. Vimonses, V.; Jin, B.; Chow, C.W.K.; Saint, C. An adsorption-photocatalysis hybrid process using multi-functional-nanoporous materials for wastewater reclamation. *Water Res.* **2010**, *44*, 5385–5397. [\[CrossRef\]](#) [\[PubMed\]](#)
45. Brahimi, B.; Mekatel, E.; Mellal, M.; Baaloudj, O.; Brahimi, R.; Hemmi, A.; Trari, M.; Belmedani, M. Enhanced photodegradation of acid orange 61 by the novel hetero-junction $\text{CoFe}_2\text{O}_4/\text{AgCl}$. *Opt. Mater.* **2021**, *121*, 111576. [\[CrossRef\]](#)
46. Belabed, C.; Tab, A.; Belhamdi, B.; Boudiaf, S.; Bellal, B.; Benrekaa, N.; Trari, M. Optical and dielectric properties of polyaniline- ZnO nanoparticles for enhancing photodegradation of organic pollutants. *Optik* **2021**, *248*, 168066. [\[CrossRef\]](#)
47. Baaloudj, O.; Nasrallah, N.; Bouallouche, R.; Kenfoud, H.; Khezami, L.; Assadi, A.A. High efficient Cefixime removal from water by the sillenite $\text{Bi}_{12}\text{Ti}_{20}$: Photocatalytic mechanism and degradation pathway. *J. Clean. Prod.* **2022**, *330*, 129934. [\[CrossRef\]](#)

48. Belabed, C.; Tab, A.; Moulai, F.; Černohorský, O.; Boudiaf, S.; Benrekaa, N.; Grym, J.; Trari, M. ZnO nanorods-PANI heterojunction dielectric, electrochemical properties, and photodegradation study of organic pollutant under solar light. *Int. J. Hydrogen Energy* **2021**, *46*, 20893–20904. [[CrossRef](#)]
49. Belabed, C.; Tab, A.; Bellal, B.; Belhamdi, B.; Benrakaa, N.; Trari, M. High photocatalytic performance for hydrogen production under visible light on the hetero-junction Pani-ZnO nanoparticles. *Int. J. Hydrogen Energy* **2021**, *46*, 17106–17115. [[CrossRef](#)]
50. Singu, B.S.; Srinivasan, P.; Pabba, S. Benzoyl Peroxide Oxidation Route to Nano Form Polyaniline Salt Containing Dual Dopants for Pseudocapacitor. *J. Electrochem. Soc.* **2012**, *159*, 11–18. [[CrossRef](#)]
51. Vadiraj, K.T.; Belagali, S.L. Characterization of Polyaniline for Optical and Electrical Properties Characterization of Polyaniline for Optical and Electrical Properties. *IOSR J. Appl. Chem.* **2015**, *8*, 53–56. [[CrossRef](#)]
52. Padmapriya, S.; Harinipriya, S.; Jaidev, K.; Sudha, V.; Kumar, D.; Pal, S. Storage and evolution of hydrogen in acidic medium by polyaniline. *Int. J. Energy Res.* **2017**, *42*, 1196–1209. [[CrossRef](#)]
53. Nogueira, A.E.; Lima, A.R.F.; Longo, E.; Leite, E.R.; Camargo, E.R. Structure and photocatalytic properties of Nb-doped Bi₁₂TiO₂₀ prepared by the oxidant peroxide method (OPM). *J. Nanoparticle Res.* **2014**, *16*, 2653. [[CrossRef](#)]
54. Li, W.; Wang, J.; He, G.; Yu, L.; Noor, N.; Sun, Y.; Zhou, X.; Hu, J.; Parkin, I.P. Enhanced adsorption capacity of ultralong hydrogen titanate nanobelts for antibiotics. *J. Mater. Chem. A* **2017**, *5*, 4352–4358. [[CrossRef](#)]
55. Wang, L.; Shi, C.; Pan, L.; Zhang, X.; Zou, J.J. Rational design, synthesis, adsorption principles and applications of metal oxide adsorbents: A review. *Nanoscale* **2020**, *12*, 4790–4815. [[CrossRef](#)]
56. Omrani, N.; Nezamzadeh-Ejehieh, A. A ternary Cu₂O/BiVO₄/WO₃ nano-composite: Scavenging agents and the mechanism pathways in the photodegradation of sulfasalazine. *J. Mol. Liq.* **2020**, *315*, 113701. [[CrossRef](#)]
57. Benamira, M.; Lahmar, H.; Messaadia, L.; Rekhila, G.; Akika, F.Z.; Himrane, M.; Trari, M. Hydrogen production on the new hetero-system Pr₂NiO₄/SnO₂ under visible light irradiation. *Int. J. Hydrogen Energy* **2020**, *45*, 1719–1728. [[CrossRef](#)]
58. Bessekhoud, Y.; Brahimi, R.; Hamdini, F.; Trari, M. Cu₂S/TiO₂ heterojunction applied to visible light Orange II degradation. *J. Photochem. Photobiol. A Chem.* **2012**, *248*, 15–23. [[CrossRef](#)]
59. Balakumar, V.; Ramalingam, M.; Sekar, K.; Chuaicham, C.; Sasaki, K. Fabrication and characterization of carbon quantum dots decorated hollow porous graphitic carbon nitride through polyaniline for photocatalysis. *Chem. Eng. J.* **2021**, *426*, 131739. [[CrossRef](#)]

Disclaimer/Publisher's Note: The statements, opinions and data contained in all publications are solely those of the individual author(s) and contributor(s) and not of MDPI and/or the editor(s). MDPI and/or the editor(s) disclaim responsibility for any injury to people or property resulting from any ideas, methods, instructions or products referred to in the content.